Practical Current Derivation Method for a Highly Accurate Variable Switching Frequency ZVS regulation in TCM operated Bidirectional Buck/Boost Converters

Bryan Gutierrez, Zhengming Hou, Dong Jiao, Jih-Sheng Lai
Future Energy Electronics Center
Virginia Tech
Blacksburg, VA, USA
Email: bryangs@vt.edu

***Abstract*— Triangular conduction mode (TCM) is a technique to operate non-isolated buck/boost converters under zero voltage switching (ZVS) turn-on. In TCM, a negative current is required for the active device to turn on under ZVS condition. The magnitude of this current is well-known and established. However, the derivation of the variable switching frequency according to the operating condition is usually simplified with the linear character of the magnetization and demagnetization of the inductors in the converter. The utilization of this simplification can increase the peak-to-peak current ripple in the inductor and burden the duty cycle loss in the controller. Additionally, it can increase the turn-off loss in the devices. This paper presents a highly accurate computation for the variable switching frequency to reduce the negative effects of the simplified method. Derivations are presented for charging and discharging modes, and they were tested in a 15-kW rated bidirectional dual-phase buck-boost converter.**

Keywords*— *bidirectional dc-dc converter, triangular conduction mode (TCM), variable switching frequency, zero-voltage switching (ZVS).

I. INTRODUCTION

Resonant dc-dc converters such as the LLC converter have been popularly adopted in industries because of its distinctive advantages such as galvanic isolation, zero-voltage switching (ZVS), and zero-current switching (ZCS) under certain operating conditions. However, they are not suitable for off-board fast chargers of electric vehicles because of its limited wide range input to output voltage gain [1]. Consequently, a two-stage structure that implements a constant-gain LLC stage as a highly-efficient galvanic isolation dc transformer (DCX) with an added non-isolated bidirectional buck/boost stage that allows ZVS operation has gained attention for fast charging applications [2].

To reduce the switching losses that normally occur in the continuous conduction mode (CCM) of bidirectional buck/boost converters, several techniques such as synchronous conduction mode (SCM), critical conduction mode (CRM), and triangular conduction mode (TCM) have been developed [3]-[5]. TCM comes ahead because it can achieve ZVS turn-on in the active device without depending on the input-to-output voltage ratio [6], [7]. Additionally, its inherited variable switching frequency (VSF) can ease the stress in the inductor, which can further reduce the magnetic losses of the converter. Typically, to obtain the VSF, a simplified linearized model of the inductor is used. However, this simplification can affect the duty cycle controller, cause loss of ZVS and increase the magnetic component losses.

This paper presents an accurate derivation for the VSF to achieve precise ZVS under TCM condition by considering the resonant model of the inductor along with the device output capacitance for the non-isolated bidirectional buck/boost dc-dc converter. Overall, the presented practical current derivations maintain a low but sufficient current to achieve ZVS turn-on. It can also match the resonance duration with the required dead time. Compared to the simplified model, the presented method minimizes the current swing associated device conduction, turn-off and inductor losses, thus achieving ultrahigh power conversion efficiency over a wide range of voltage and load conditions. The derivations were verified experimentally in a high-power-density 15 kW dual-phase interleaved buck/boost converter.

II. THE BIDIRECTIONAL BUCK/BOOST CONVERTER AND ITS TCM OPERATING PRINCIPLE

The basic structure of the bidirectional synchronous buck/boost converter is depicted in Fig. 1 (a), where V_{batt}, I_{batt},

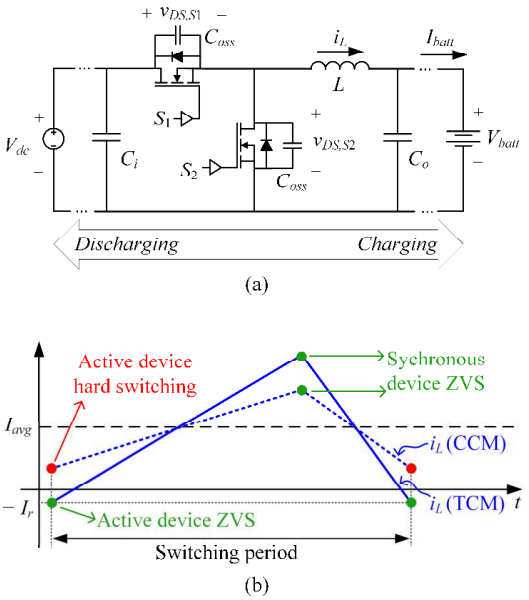

Fig. 1. (a) Bidirectional buck/boost dc-dc converter. (b) typical inductor waveforms under CCM and TCM.

and V_{dc} are sensed values by the controller. This dc-dc converter can naturally achieve ZVS turn-on for its low-side device (S_2) and its high-side device (S_1), when operating in charging mode (buck) and discharging mode (boost), respectively. This is because the magnitude of current in the inductor is the highest at the turn-on instant, which can rapidly discharge the output capacitance of the device (C_{oss}) without requiring a long dead time.

The naturally ZVS turn-on device is identified as the synchronous device, while its complimentary side is called the active device (S_1 for buck, and S_2 for boost). Despite its ZVS capability, the synchronous device still suffers from a high turn-off loss, which can be mitigated by lowering the level of its current at the commutation instant. On the other hand, the C_{oss} in the active device cannot be discharged when the converter is operated in conventional CCM because of the inductor's current polarity, causing hard switching turn-on in the active device as seen in Fig. 1 (b). Thus, applying the TCM principle, the active device can achieve ZVS turn-on by forcing a reverse current ($-I_r$) flowing at the turn-on instant. As a result, the C_{oss} can be discharged during the dead time (T_d) before the active device is turned on. However, if I_r is too large, the turn-off switching loss in the active device increases. Additionally, if T_d is too long, C_{oss} discharges first, and the remaining time the device continues in reverse conduction mode, which increases the conduction loss. Therefore, a variable switching frequency scheme is implemented in TCM to reduce the device's reverse conduction loss and turn-off switching loss by computing an I_r low enough to match the C_{oss} discharge time during T_d.

III. Practical Computations for Variable Switching Frequency TCM

A. TCM Characteristic Waveforms

Fig. 2 depicts the practical waveforms of the commutations during a switching period (T_{sw}) for both buck- and boost-mode operations for the bidirectional dc-dc converter. The current waveform can be divided into four stages: (a) slow resonant stage (SRS), (b) fast resonant stage (FRS), (c) magnetizing linear stage (MLS), and (d) demagnetizing linear stage (DMLS). Conventionally, the current waveform is approximated using the MLS and DMLS when operating in CCM without ZVS turn-on in the active switch. This linear approach has also been implemented successfully for TCM, yet, as it will be presented, this simplification can affect the core and winding losses of the inductor, increase the reverse conduction loss of the active device, and increase the turn-off losses of both devices. For the buck-mode case in Fig. 2 (a), the SRS starts when $-I_r$ is reached, and the synchronous device gate is turned off. During T_d, the inductor's current waveform is given by

$$i_{SRS}(t) = I_r \cos(\omega_o t) + V_{batt} \sin(\omega_o t) / Z_o \quad (1)$$

where ω_o and Z_o are the resonant frequency and the characteristic impedance of the resonant tank formed by L and C_{oss}, which are given by

$$\omega_o = 1/\sqrt{2LC_{oss}} \quad (2)$$

$$Z_o = \sqrt{L/(2C_{oss})}. \quad (3)$$

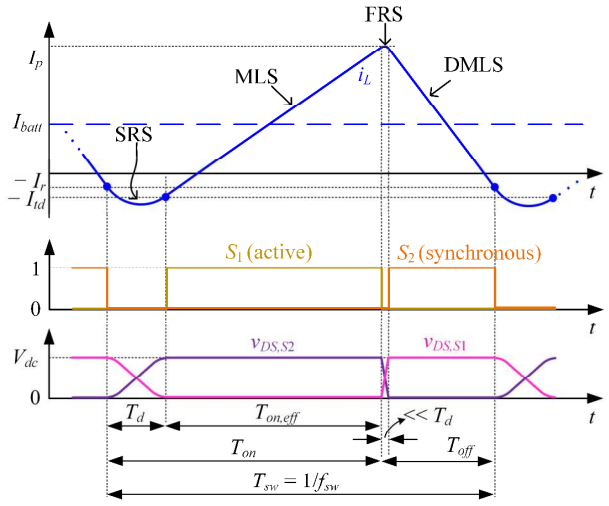

(a)

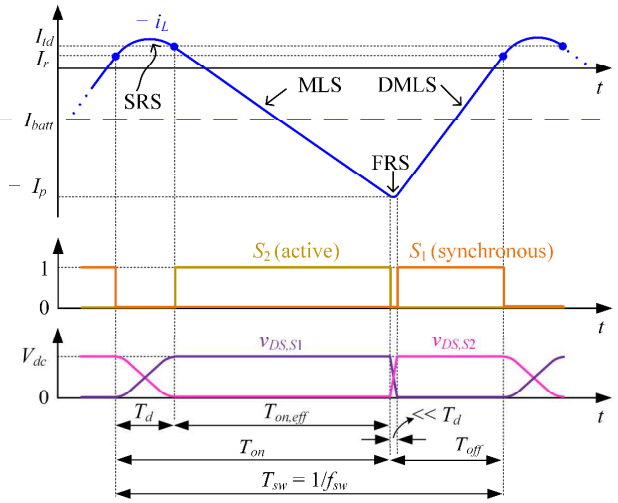

(b)

Then, the MLS and DMLS stages are governed by the following well-known expressions:

$$i_{MLS}(t) = t(V_{dc} - V_{batt})/L \quad (4)$$

$$i_{DMLS}(t) = -tV_{batt}/L. \quad (5)$$

Finally, the FRS is analogous to (1), however, the duration of this stage is regarded as negligible because the positive peak current (I_p) is considerably large to quickly achieve ZVS turn-on, which requires a dead time much smaller than T_d.

As mentioned in the previous section, I_r should be as low as possible to avoid a large current ripple in the inductor which yields increased core and winding losses. Also, an unnecessarily large I_r increases the turn-off loss in the active device and can increase the duration of its reverse conduction loss. To determine the minimum value of I_r, the stored charge distribution of C_{oss} in (6) must equal the charge transferred from the inductor during T_d in (7), yielding the optimal I_r for the buck case in (8). [7]

$$Q_C = 2V_{dc}C_{oss} \quad (6)$$

$$Q_L = \int_0^{T_d} i_{SRS}(t).dt \quad (7)$$

$$I_r = \frac{V_{dc} - V_{batt}\left[1-\cos(\omega_o T_d)\right]}{Z_r \sin(\omega_o T_d)}. \tag{8}$$

If the deadtime T_d is selected as a very small value, (8) yields a large I_r (renamed as $I_{r'}$ for a small dead time in Fig. 3 (a)). Consequently, the SRS turns into FRS, thus, the linear method with MLS and DMLS can be sufficient to meet the designed $I_{r'}$ and the new switching frequency ($f_{sw'} = 1/T_{sw'}, f_{sw'} < f_{sw}$), as observed in Fig. 3 (a) for buck mode [7]-[9]. Notice that the resulting inductor's current waveform ($i_{L'}$) with the simplified method also has its positive peak current ($I_{p'}$) increased. Thus, the utilization of a small dead time and its resulting large $I_{r'}$ and $I_{p'}$ increases losses in the magnetic components and semiconductor devices as previously explained. Conversely, if an adequate dead time is designed to yield sufficiently small I_r, the linear simplification could incur into errors and restrict the range operation of the controller. To illustrate this issue, Fig. 3 (b) shows $i_{L,ctrl}$, which is the ideal shape of the inductor waveform seen from the controllers perspective when operated with the linear approximation. Thus, its MLS and DMLS correspond to the on-state of S_1 and S_2, respectively. Although $I_{batt,ctrl} = I_{batt}$ to try keep track of the reference by the controller, the actual waveform $i_{L''}$ has a battery current ($I_{batt''}$) lower than the reference. As a result, the CC or VC responds increasing the duty cycle by Δd to obtain the same $I_{batt} = I_{batt''}$, which can increase the duty cycle loss. Additionally, $i_{L''}$ has $I_{p''}$ reduced, which turns the stage from FRS into SRS, therefore, ZVS can be lost in this stage because the dead time in this stage is shorter than T_d.

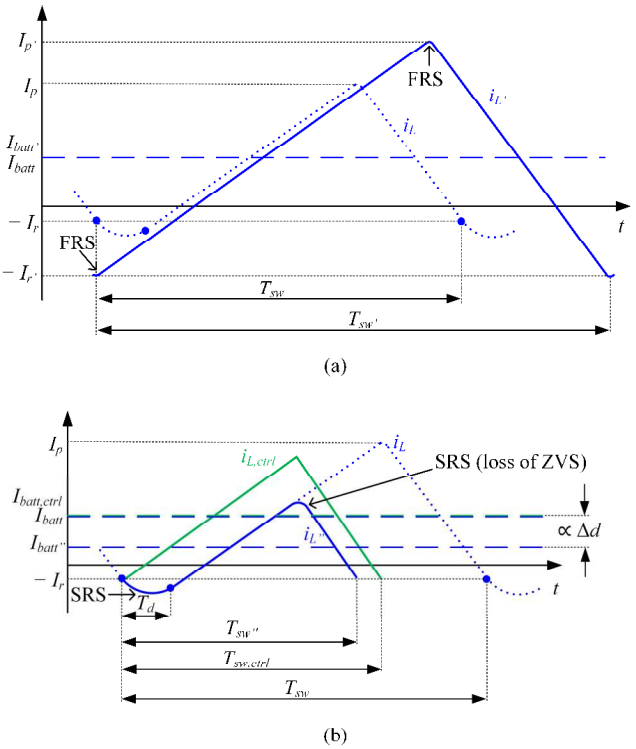

Fig. 3. Magnified effects of the simplified method vs. the proposed practical method. (a) When dead time is very small. (b) When dead time is long enough.

B. *Proposed Practical Method*

Based on the average inductor current, which is measured as I_{batt}, the proposed practical method can accurately calculate the minimum I_r to have ZVS achieved after T_d, which can eliminate the reverse conduction loss in the device during the dead time. With the average current in each stage: SRS, MLS, and DMLS, an accurate model of VSF for ZVS can be achieved. Considering first the buck or charging mode of the dc-dc converter, the average current in SRS, MLS, and DMLS, are given by (9), (10), and (11), respectively.

$$I_{SRS} = \frac{1}{T_d}\int_0^{T_d} i_{SRS}(t).dt \tag{9}$$

$$I_{MLS} = \frac{I_P - I_{td}}{2} \tag{10}$$

$$I_{DMLS} = \frac{I_P - I_r}{2}. \tag{11}$$

Next, the variable I_p can be computed by equating the sum of (9), (10), and (11) to the periodic average I_{batt}. Thus, I_p is found in (12), where d is the duty cycle given by the current controller (CC) or voltage controller (VC) of the bidirectional converter. Then the timing durations of the SRS, MLS, and DMLS, are calculated from (13), (14), and (15), which are used to calculate the required switching frequency in (16).

$$T_{SRS} = T_d \tag{13}$$

$$T_{MLS} = L\frac{I_P + I_{td}}{V_{dc} - V_{batt}} \tag{14}$$

$$T_{DMLS} = L\frac{I_P + I_r}{V_{batt}} \tag{15}$$

$$f_{sw} = \frac{1}{T_{SRS} + T_{MLS} + T_{DMLS}} \tag{16}$$

In a similar manner, the VSF expressions for the buck or discharging mode of the dc-dc converter are calculated as follow following expressions from (17) to (21).

$$T_{SRS} = T_d \tag{18}$$

$$T_{MLS} = L\frac{I_P + I_{td}}{V_{batt}} \tag{19}$$

$$T_{DMLS} = L\frac{I_P + I_r}{V_{dc} - V_{batt}} \tag{20}$$

$$I_p = \frac{2I_{batt} - d\left(I_r - I_{td}\right) - T_d f_{sw} I_{td} + I_r + 2f_{sw}\left(I_r \sin(\omega_o T_d) + V_{batt}\sin(\omega_o T_d)/Z_r\right)/\omega_o}{1 - T_d f_{sw}} \tag{12}$$

$$I_p = \frac{2I_{batt} - d\left(I_r - I_{td}\right) - T_d f_{sw} I_{td} + I_r + 2f_{sw}\left(I_r \sin(\omega_o T_d) + (V_{dc} - V_{batt})\sin(\omega_o T_d)/Z_r\right)/\omega_o}{1 - T_d f_{sw}} \tag{17}$$

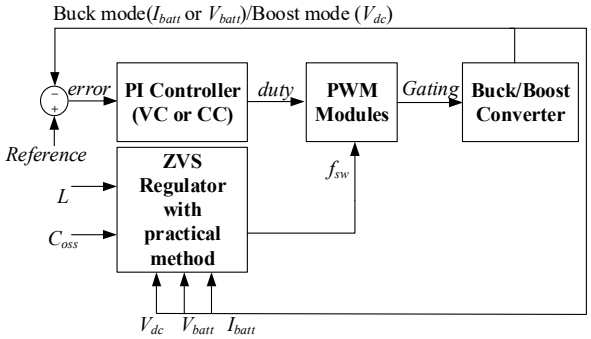

Fig. 4. Block diagram controller for the bidirectional dc-dc converter with the proposed practical method for TCM.

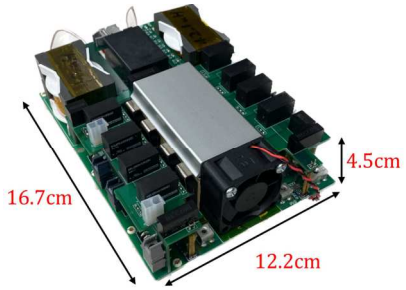

Fig. 5. Prototype of the 15-kW non-isolated bidirectional dc-dc buck/boost converter.

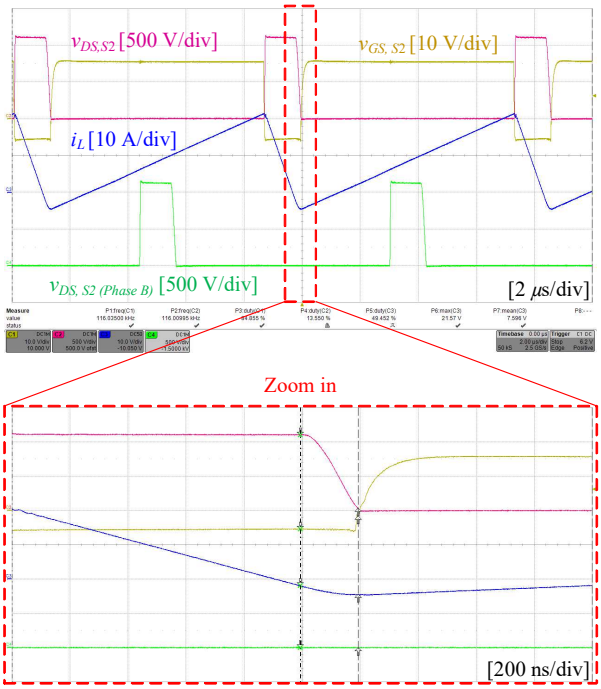

Fig. 6. Experimental verification of the practical method TCM in the prototype presented in Fig. 5. Boost/discharging operation (V_{dc} = 1100 V, V_{batt} = 150 V).

TABLE I
EXPERIMENTAL SETUP AND PROTOTYPE PARAMETERS

Parameter	Value/Model
MOSFETs	G3R45M17K
MOSFET output capacitance (C_{oss})	330 pF @ 1100 V
Inductor (L)	42 μH
Deadtime (T_d)	200 ns
Range of switching frequency (f_{sw})	80 kHz ~ 350 kHz
Rated dc-link voltage (V_{dc})	1100 V
Range of battery/load voltage (V_{batt})	150 V ~ 1000 V
Maximum battery/load current ($I_{batt,max}$)	25 A
Rated Power	15 kW
Charging mode peak efficiency	99.815
Discharging mode peak efficiency	99.821
Power density	16.36 kW/L

TABLE II
MEASURED AND CALCULATED VALUES OF THE PRACTICAL METHOD OPERATING IN BOOST/DISCHARGING

Item	Calculated	Measured	Condition
I_p (A)	21.33	21.486	
Ir (A)	2.445	2.11	V_{batt} = 150 V
I_{td} (A)	4.5	4.477	
I_p (A)	19.21	19.75	
Ir (A)	2.49	2.33	V_{batt} = 170 V
I_{td} (A)	4.456	4.56	
I_p (A)	12.87	12.75	
Ir (A)	2.83	2.931	V_{batt} = 300 V
I_{td} (A)	4.11	4.245	
I_p (A)	10.53	10.426	
Ir (A)	3.13	3.09	V_{batt} = 420 V
I_{td} (A)	3.81	3.904	

$$f_{sw} = \frac{1}{T_{SRS} + T_{MLS} + T_{DMLS}} \tag{21}$$

Notice that the difference comes from the MLS and DMLS timing expressions, which utilize a different I_p expression in the boost mode.

IV. EXPERIMENTAL VALIDATION

The controller was implemented in the TMS320F28377D digital signal processor (DSP) where the CC and VC linear compensators where implemented at a rate of 10 μs. Also, the proposed practical method was implemented in the DSP as a ZVS regulation stage that outputs the required switching frequency to the PWM modules at a rate of 1 ms. The overall block diagram of the control structure is presented in Fig. 4, where the bidirectional operation is enabled by CC and VC in both charging and discharging modes.

The proposed technique was verified with an in-house built high-power density 15 kW dual phase interleaved non-isolated buck/boost converter as shown in Fig. 5. The salient features and parameters of the experimental prototype are listed in Table I [10]. To control the two phases of this prototype, the scheme in Fig. 4 is separated into two PWM channels 180° apart. Also, the measured average battery current is halved to calculate expressions (12) and (17) in each leg of the dual phase ZVS regulator.

One phase of the converter is probed to verify the accuracy of the proposed practical method in Fig. 6, where V_{dc} = 1100 V and V_{batt} = 150 V in boost/discharging mode with VC. As seen in zoomed Fig. 6 (b), ZVS is exactly achieved by the end of the dead time T_d = 200 ns, avoiding reverse conduction loss

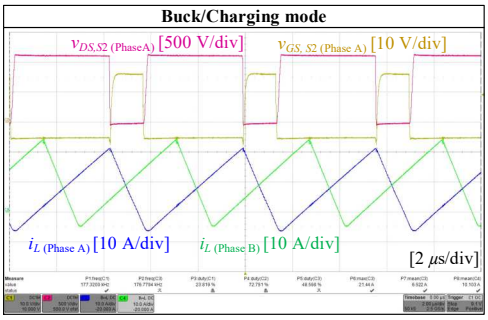

(a)

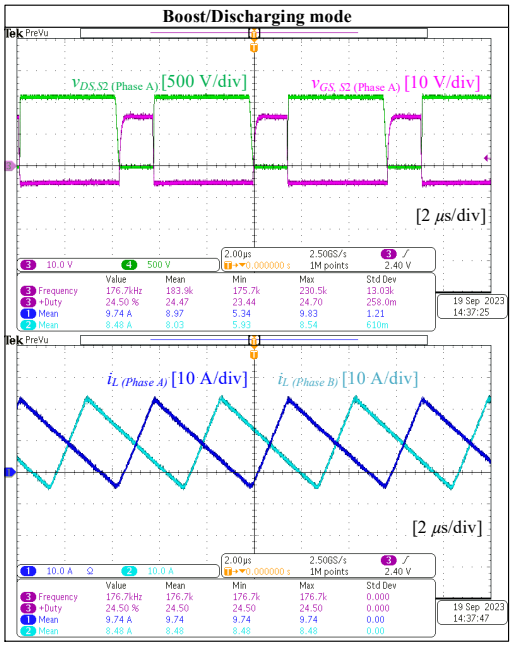

(b)

Fig. 7. 15-kW operation of the dual-phase dc-dc bidirectional converter with V_{dc} = 1100 V, V_{batt} = 600 V, and I_{batt} =25 A. (a) Waveforms under buck or charging mode. (b) Waveforms under boost or discharging mode.

in the device. While Fig. 6 is a telltale of the accuracy of the proposed method by matching T_d to the gate turn-on signal, Table II compares the calculated and measured peak current I_p, reverse current I_r, and the current at the end of dead time I_{td} under different operating conditions. Both calculated and measured values are well matched. As a result, the losses are minimized, and ultrahigh efficiency was achieved. As shown in Table I, under both buck and boost modes, the peak efficiency exceeds 99.8% at the full power of 15 kW. Note that the maximum efficiency occurs at V_{batt} = 1000 V because of the smallest inductor currents.

The full power operation of the dual-phase bidirectional dc-dc converter is verified in Fig. 7. Two of these converters were implemented and connected back-to-back in a regenerative testing setup that allows for accurate measurements of efficiency while having both modes (charging and discharging) operating simultaneously [11]. Two separate oscilloscopes were used to measure the gating and inductor waveforms. Fig. 7(a) depicts the measured waveforms for the buck or charging mode converter with one oscilloscope. Fig. 7(b) depicts the measured waveforms for the boost or discharging mode converter with another oscilloscope. Both operating modes are showing stable operation under 15-kW full-power output condition. Also, as previously seen in Fig. 6, the ZVS in the active switches is clearly shown as the drain-to-source voltage falls before the increase of the gate-to-source voltage in the boost mode. The test condition in Fig. 7 represents the maximum battery current under full-power operating condition. Measured efficiency were 99.45% under buck mode condition and 99.48% under boost mode condition.

V. Conclusion

A practical method to accurately calculate the variable frequency in TCM was presented in this paper. The method helps keep a low negative current for ZVS turn-on in the active devices while aiding in the reduction of current ripples to reduce losses in the inductor. Additionally, it can closely match the dead time to avoid reverse conduction losses. The derivations were presented for the buck and boost modes of the bidirectional dc-dc converter. The proposed technique was verified in a high-power-density 15-kW bidirectional buck/boost converter with two interleaved phases. With the proposed precise ZVS condition calculation, the full-load efficiency under maximum battery charging current condition exceeds 99.4% under both operating modes, and the peak efficiency under maximum battery voltage condition exceeds 99.8%.

Acknowledgment

This work was supported by the Industrial Technology Research Institute (ITRI), Taiwan.

References

[1] X. Wu and H. Shi, "High efficiency high density 1 MHz 380−12V DCX with low FoM devices," *IEEE Trans. on Ind. Electron.*, vol. 67, no. 2, pp. 1648-1656, Feb. 2020.

[2] F. Liu, X. Ruan, and Y. Jiang, "Resonant peak suppression approaches for improving the dynamic performance of DCX-LLC resonant converter based two-stage dc-dc converter," *IEEE Trans. on Ind. Electron.*, vol. 70, no. 6, pp. 5685-5695, Jun. 2023.

[3] C.-S. Yeh, O. Yu, X. Zhao, and J.-S. Lai, "Dual-loop controlled couple-inductor buck converter in low-power applications," *IEEE Open Journal of Power Electronics*, vol. 1, pp. 24-33, 2020

[4] C.-S. Yeh, X. Zhao, and J.-S. Lai, "An investigation on zero-voltage-switching condition in synchronous-conduction-mode buck converter," *in Proc. IEEE Energy Convers. Congr. Expo. (ECCE)*, Cincinnati, OH, USA, Oct. 2017, pp. 1728-1732.

[5] D. Sha, Y. Zhao, and D. Zhang, "ZVS-interleaved synchronous buck dc-dc converter with a coupled inductor by varying switching frequency and deadtime," *IEEE Trans. on Power Electron.*, vol. 37, no. 7, pp. 8190-8198, July 2022.

[6] A. Vazquez, K. Martin, M. Arias, and J. Sebastian, "Variable-width hysteretic analog control for QSW-ZVS TCM source/sink converters," *IEEE Trans. on Power Electron.*, vol. 35, no. 3, pp. 3195-3207, Mar. 2020.

[7] Y.-C. Liu, *et al.*, "High-switching-frequency TCM digital control for bidirectional-interleaved buck converters without phase error for battery charging," *IEEE J. Emerg. Sel. Topics Power Electron.*, vol. 8, no. 3, pp. 2111-2123, Sept. 2020.

[8] J.-B. Baek, W.-I. Choi, and B.-H. Cho, "Digital adaptive frequency modulation for bidirectional dc-dc converter," *IEEE Trans. on Ind. Electron.*, vol. 60, no. 11, pp. 5167-5176, Nov. 2013.

[9] Q. Huang and A. Q. Huang "Variable frequency average current mode control for ZVS symmetrical dual-buck H-bridge all-GaN inverter," *IEEE J. Emerg. Sel. Topics Power Electron.*, vol. 8, no. 4, pp. 4416-4427, Sept. 2020.

[10] Z. Hou, D. Jiao, B. Gutierrez, J.-S. Lai, and P.-L. Chen, "Design of a 15-kW high-efficiency and high-power density bidirectional TCM buck/boost converter," *in Proc. IEEE Appl. Power Electron. Conf. Expo. (APEC)*, Long Beach, CA, USA, Feb. 2024.

[11] W. Yu, H. Qian, and J.-S. Lai, "Design of high-efficiency bidirectional dc-dc converter and high-precision efficiency measurement," *Trans. Power Electron.*, vol. 25, no. 3, pp. 650-658, Mar. 2010.